

See discussions, stats, and author profiles for this publication at: <https://www.researchgate.net/publication/276377848>

Perovskite Solar Cells: Beyond Methylammonium Lead Iodide

ARTICLE *in* JOURNAL OF PHYSICAL CHEMISTRY LETTERS · FEBRUARY 2015

Impact Factor: 7.46 · DOI: 10.1021/jz502547f

CITATIONS

15

READS

89

5 AUTHORS, INCLUDING:



Pablo P. Boix

Nanyang Technological University

59 PUBLICATIONS 1,879 CITATIONS

[SEE PROFILE](#)



Shweta Agarwala

Nanyang Technological University

24 PUBLICATIONS 246 CITATIONS

[SEE PROFILE](#)



Teck Ming Koh

Nanyang Technological University

46 PUBLICATIONS 368 CITATIONS

[SEE PROFILE](#)



Subodh G Mhaisalkar

Nanyang Technological University

383 PUBLICATIONS 8,418 CITATIONS

[SEE PROFILE](#)

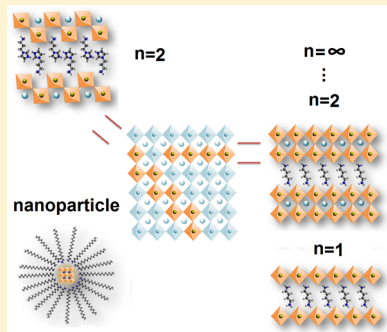
Perovskite Solar Cells: Beyond Methylammonium Lead Iodide

Pablo P. Boix,*[†] Shweta Agarwala,[†] Teck Ming Koh,[†] Nripan Mathews,^{†,‡} and Subodh G. Mhaisalkar*,^{†,‡}

[†]Energy Research Institute at Nanyang Technological University (ERI@N), Research Techno Plaza, X-Frontier Block Level 5, 50 Nanyang Avenue, Singapore 637553, Singapore

[‡]School of Materials Science and Engineering, Nanyang Technological University, 50 Nanyang Avenue, Singapore 639798, Singapore

ABSTRACT: Organic–inorganic lead halide based perovskites solar cells are by far the highest efficiency solution-processed solar cells, threatening to challenge thin film and polycrystalline silicon ones. Despite the intense research in this area, concerns surrounding the long-term stability as well as the toxicity of lead in the archetypal perovskite, $\text{CH}_3\text{NH}_3\text{PbI}_3$, have the potential to derail commercialization. Although the search for Pb-free perovskites have naturally shifted to other transition metal cations and formulations that replace the organic moiety, efficiencies with these substitutions are still substantially lower than those of the Pb-perovskite. The perovskite family offers rich multitudes of crystal structures and substituents with the potential to uncover new and exciting photophysical phenomena that hold the promise of higher solar cell efficiencies. In addressing materials beyond $\text{CH}_3\text{NH}_3\text{PbI}_3$, this Perspective will discuss a broad palette of elemental substitutions, solid solutions, and multidimensional families that will provide the next fillip toward market viability of the perovskite solar cells.



Perovskites that exhibit the simple AMX_3 (cations, A; metal, M; anion, X; Figure 1a) base configuration have the propensity for rich diversity in composition, structure, and properties. Perovskite minerals in the form of oxides, nitrides, and halides with their unique ferro- and piezoelectric, colossal magnetoresistive, superconducting, semiconducting, and catalytic properties have been a cornerstone of high-performance materials for solid-state devices such as capacitors, actuators, transducers, and optical modulators.^{1,2} Over the past century, these materials have been the mainstay of research in inorganic materials with loparite, silicates, spinels, and with layered Aurivillius and Ruddlesden–Popper phases receiving much attention. However, interest in these materials for photovoltaics has soared due to reports of efficient light harvesting and lasing in organometallic halides, represented by methylammonium lead iodide ($\text{CH}_3\text{NH}_3\text{PbI}_3$) and its analogues. Within a span of two years, this organic–inorganic lead halide perovskite has yielded photovoltaic efficiencies of 20.1%,³ being the highest-performing solution-processed solar cell on record and displacing technologies such as dye solar cells and organic photovoltaics that were showing signs of inertia after two decades of intensive research (Figure 1b).

The fundamental properties that have wrought this success include a sharp band gap close to the ideal, high absorbance⁴ (Figure 1c), low exciton binding energy⁵ with the excited state composed primarily of free carriers⁶ (Figure 1d), near perfect crystalline film formation with very low defect densities, balanced electron–hole transport^{7,8} (Figure 1e) and excellent charge carrier mobilities. These characteristics that bear similarities to the gold standards of crystalline silicon and GaAs, support the conjecture that the perovskite solar cells will continue to scale new heights in efficiencies, applications, and device integration. Compatibility of the perovskites with

materials used in dye solar cells and organic photovoltaics also enable investigation of a wide variety of device architectures. Much of the research in perovskite solar cells focus on new materials for functional interfaces^{9–11} (organic, inorganic and carbon based hole transport materials (HTMs)), device architectures^{12,13} (mesoscopic, planar), and innovative fabrication processing methodologies^{12,14,15} (vapor phase transformations, single step and sequential depositions, solvent annealing). Power conversion efficiencies have been enhanced primarily through improved processing conditions which reduce losses within the solar cell; with $\text{CH}_3\text{NH}_3\text{PbI}_3$ being common material of interest for the vast majority of reports.

It is however evident that nontoxic alternatives to lead in $\text{CH}_3\text{NH}_3\text{PbI}_3$ are necessary for their market acceptance. Additionally, the tetragonal structure of $\text{CH}_3\text{NH}_3\text{PbI}_3$ undergoes a phase transition to cubic structure at 330 K (Figure 1f), a temperature achievable under practical conditions for an installed photovoltaic array,¹⁶ which adds to the concerns about the ambient stability of this material.

The necessary pursuit of alternatives beyond $\text{CH}_3\text{NH}_3\text{PbI}_3$ thus essentially begins with understanding the basic tenets of this material.

Received: December 3, 2014

Accepted: February 13, 2015

Published: February 13, 2015

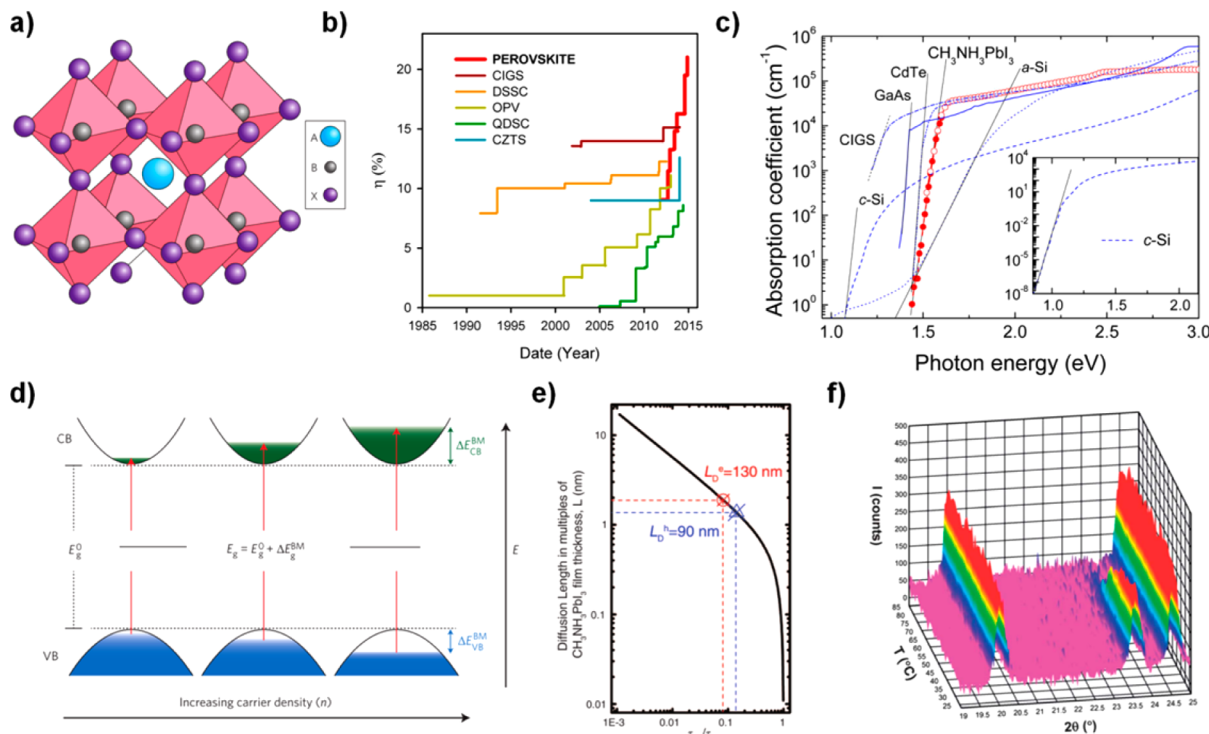


Figure 1. (a) Schematic crystal structure of AMX_3 perovskites. Reprinted with permission from ref 17. (b) Solar conversion efficiency progress for solution-processed solar cells. (c) Effective absorption coefficient of a $\text{CH}_3\text{NH}_3\text{PbI}_3$ perovskite thin film compared to other typical photovoltaic materials, including amorphous silicon (a-Si), GaAs, CIGS, CdTe, and crystalline silicon (c-Si), all measured at room temperature with the slope of the Urbach tail indicated. The inset shows the data for c-Si down to low absorption values. Reprinted with permission from ref 4. (d) Schematic representation of the Burstein–Moss effect showing the contribution from both electrons in the conduction band (CB) and holes in the valence band (VB) due to their similar effective masses reprinted with permission from ref 6. (e) Electron and hole diffusion lengths in perovskite solar cells versus transient PL decay ratios. Reprinted with permission from ref 7. (f) Phase transition: expanded powder X-ray diffraction patterns for $\text{CH}_3\text{NH}_3\text{PbI}_3$ which show the gradual disappearance of the 211 reflection associated with the tetragonal super cell. Reprinted with permission from ref 16.

The necessary pursuit of alternatives beyond $\text{CH}_3\text{NH}_3\text{PbI}_3$ thus essentially begins with understanding the basic tenets of this material, including the AMX_3 perovskite structure formed with a three-dimensional (3-D) network of corner-sharing MX_6 octahedra and the A cation occupying the cuboctahedral cavity maintaining the electronegativity of the system. Exploration of alternatives to $\text{CH}_3\text{NH}_3\text{PbI}_3$ could thus be classified based on substitutions at the A, M, and X positions. These would include halide substitution (Figure 2a), monovalent cation and divalent metallic substitutions (Figure 2b and c). Multilayered structures of perovskites are also made possible by alternating organic molecules between the neighboring perovskite sheets. Tuning the organic layers by controlling the size of the cations and altering the ratio of the A and MX_6 constituents can yield to multidimensional perovskites with a controlled inorganic layer stacking, (n ; Figure 2d). These allow for a wider compositional flexibility and represent the greatest potential to yield disruptive performances not only in solar cells but also in light emitting diodes, printable electronics, spintronics, and other emergent electronics.

Topics such as process engineering for improved efficiency, exciton dynamics, and interfaces have been topics of previous reports.^{5,15,18} This article instead will emphasize the materials considerations and related properties of multidimensional metal organic halides, hybrid perovskites, and other perovskite families that hold promise of green, high efficiency photovoltaics.

Halide Substitution. The first peer-reviewed publication on perovskite solar cell²² demonstrated both $\text{CH}_3\text{NH}_3\text{PbI}_3$ and $\text{CH}_3\text{NH}_3\text{PbBr}_3$, with the Br perovskite yielding lower efficiency. However, the larger band gap resulting from the halide-substitution can have relevant applications in fields such as tandem solar cells and light emission. The band gap of $\text{CH}_3\text{NH}_3\text{PbCl}_3$, 3.11 eV, restricts its use as a single light absorber. However, $\text{CH}_3\text{NH}_3\text{PbBr}_3$ with a 2.3 eV band gap, favorable energy levels with respect to TiO_2 , low exciton binding energy,²³ and long charge carrier diffusion lengths, have been applied in solar cells. Although these systems showed lower power conversion efficiencies, V_{oc} as high as 1.5 V was achieved on an alumina scaffold.^{24,25} This higher V_{oc} is a direct result of the higher conduction band minimum of $\text{CH}_3\text{NH}_3\text{PbBr}_3$, which forms a barrier to confine electrons and suppress back transfer recombination.²⁶ Furthermore, the charge accumulation within the perovskite²⁷ overcomes the hole Fermi level limitation by the HTM,²⁸ thus boosting the V_{oc} . An effective approach to increase the efficiency of Br-based perovskites is to synthesize mixed halide precursor solutions with varying Br content ($\text{CH}_3\text{NH}_3\text{Pb}(\text{I}_{1-x}\text{Br}_x)_3$ with $0 < x < 1$). The mixed halide system allows a band gap tuning from 786 nm (1.58 eV, for $x = 0$) to 544 nm (2.28 eV, for $x = 1$), thus exhibiting films of varying colors.²⁹ A similar result can be obtained by means of a sequential deposition process³⁰ when a PbI_2 film is dipped in a mixed $\text{CH}_3\text{NH}_3\text{I}$, $\text{CH}_3\text{NH}_3\text{Br}$ solution with simultaneous changes in band gap and morphology observed. However, the highest photovoltaic efficiencies for

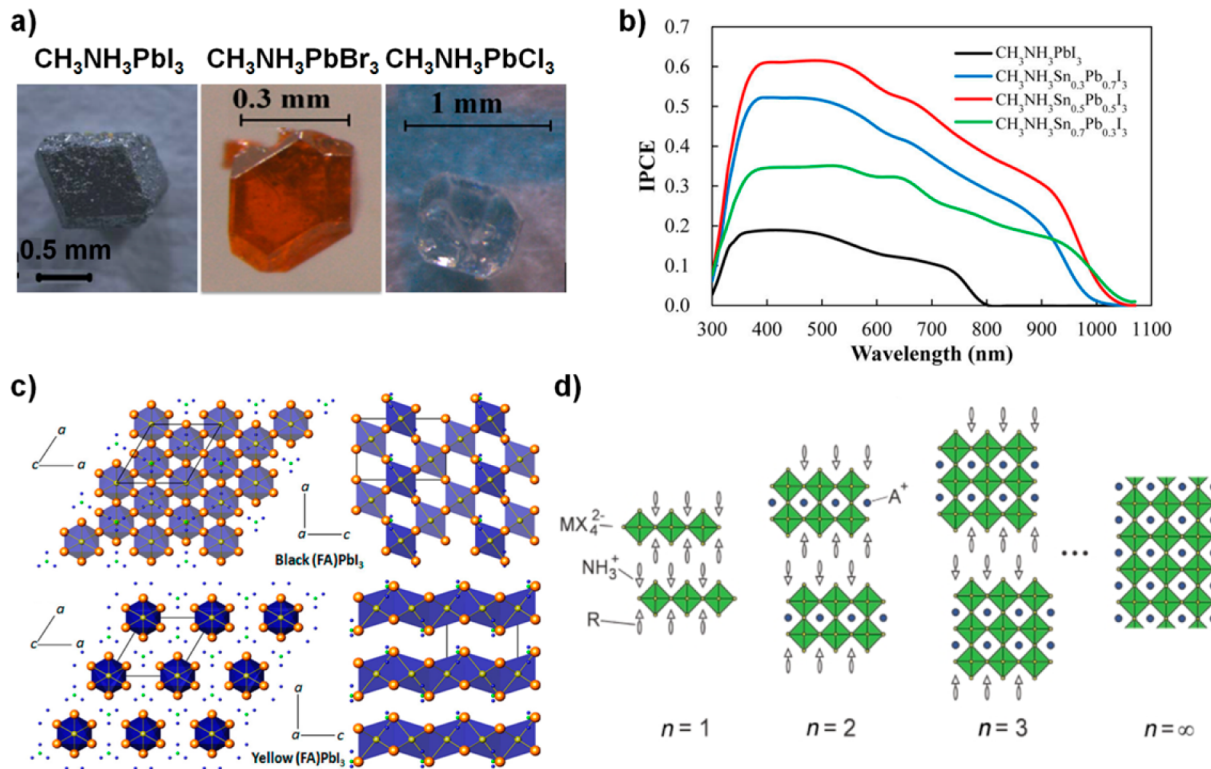


Figure 2. (a) Single crystals of $\text{CH}_3\text{NH}_3\text{PbI}_3$ (extracted from ref 16), $\text{CH}_3\text{NH}_3\text{PbBr}_3$, and $\text{CH}_3\text{NH}_3\text{PbCl}_3$. (b) IPCE characteristics of $\text{CH}_3\text{NH}_3\text{Sn}_{1-x}\text{Pb}_x\text{I}_3$ solar cells with different Sn/Pb ratio. Reprinted with permission from ref 19. (c) Schematic representation of the structures of the yellow and black FAPbI₃ polymorphs. Reprinted with permission from ref 20. (d) Stacking of inorganic octahedral layer (n) in the $\langle 100 \rangle$ -oriented 2D perovskite structure. When $n = \infty$, it is same as 3D perovskite structure. Reprinted with permission from ref 21.

$\text{CH}_3\text{NH}_3\text{PbBr}_3$ have been obtained by a solvent-engineering method, which improved the film quality in a planar solar cell configuration through inclusion of HBr in DMF solvent.³¹ Slower crystallization process achieved by reducing the evaporation rate of solvent or by increasing the solvent solubility resulted in an efficiency of 10.45%, V_{oc} 1.51 V and J_{sc} 8.4 mA cm⁻². Although the limitation in photocurrent generation is apparent, it must be noted that the record V_{oc} s result in performances close to that theoretically predicted for the band gap.

Despite the drawbacks of $\text{CH}_3\text{NH}_3\text{PbI}_3$ as an absorber, the addition of Cl to the $\text{CH}_3\text{NH}_3\text{PbI}_3$ and the possible formation of $\text{CH}_3\text{NH}_3\text{Pb}(\text{I}_{1-x}\text{Cl}_x)_3$ has been a topic of research since the initial stages of solid state perovskite solar cells.³² Although the inclusion of small amounts of Cl within the $\text{CH}_3\text{NH}_3\text{PbI}_3$ structure is theoretically feasible,³³ its effects on the optical and structural properties have not been clearly identified.⁵ However, the enhancement of the photovoltaic performances upon Cl addition,³⁴ in particular for nonconductive scaffold and thin film configurations, indicate an enhanced charge transport⁸ and reduced charge recombination.¹⁴ The origin of these effects seem to be related merely to an improved film morphology,³⁵ as it has been shown that Cl addition in the perovskite generates uniform films due to better distributed heterogeneous nucleation.³⁶ Thus, high efficiency $\text{CH}_3\text{NH}_3\text{PbI}_3$ planar solar cells can also be achieved without Cl through alternate processes such as the antisolvent addition to enable improved crystallization.^{13,37}

Although $\text{CH}_3\text{NH}_3\text{PbI}_3$ crystallizes in the tetragonal space group, the smaller ionic radius of Br^- and Cl^- , 1.96 and 1.81 Å, respectively (compared with 2.2 Å for I^-) induces the

formation of a cubic perovskite structure in $Pm\bar{3}m$ space group at room temperature.^{38,39} Although this increased symmetry is theoretically predicted to have the potential for higher photovoltaic efficiencies due to improved light absorption and electrical properties,⁴⁰ in practice, the larger band gaps of $\text{CH}_3\text{NH}_3\text{PbCl}_3$ and $\text{CH}_3\text{NH}_3\text{PbBr}_3$ make them less efficient light harvesters than $\text{CH}_3\text{NH}_3\text{PbI}_3$. However, as newer perovskite materials are developed, halide substitution could be utilized as an additional knob to control optoelectronic and morphological properties.

Metal Substitution: Toward Pb-Free Perovskite Solar Cells. As a group 14 element with comparable ionic radii, Sn was first explored as a replacement for Pb in solar cells. Previous work on organic–inorganic layered Sn perovskites⁴¹ had already demonstrated good electrical properties; however, their optoelectronic properties had remained unexplored. Partial substitution of Pb to yield $\text{CH}_3\text{NH}_3\text{Sn}_x\text{Pb}_{1-x}\text{I}_3$ ¹⁹ demonstrated that increased Sn concentration allowed for a reduced band gap; however, addition of Pb was deemed to be essential in retarding the oxidation of Sn^{2+} to Sn^{4+} , which in turn reduced carrier concentration and increased power conversion efficiencies. Highest reported photovoltaic efficiencies based on these materials were 7.37% for $\text{CH}_3\text{NH}_3\text{Sn}_{0.25}\text{Pb}_{0.75}\text{I}_3$ with low photocurrent densities being ascribed to poor perovskite film coverage on TiO_2 and the oxidation of Sn^{2+} ions ascribed as the cause of low open-circuit voltage.⁴² Enhancement of solar cell efficiencies to 10.1% was obtained with $\text{CH}_3\text{NH}_3\text{Sn}_x\text{Pb}_{1-x}\text{I}_{3-x}\text{Cl}_x$ in a planar device,⁴³ with Cl addition credited for improved film coverage, effective exciton dissociation and charge transport.

Completely lead-free perovskite solar cells based on $\text{CH}_3\text{NH}_3\text{SnI}_3$ were reported in 2014 yielding efficiencies of 5.23%⁴⁴ and 6.4%⁴⁵ with the suppression of Sn^{4+} accomplished through ultrahigh purity starting materials, fastidious synthesis and glovebox device fabrication protocols. $\text{CH}_3\text{NH}_3\text{SnI}_3$ has the advantage of reduced band gaps close to the optimum Shockley–Queisser value⁴⁶ (Figure 3a). One of the reports demonstrated an open-circuit voltage of 0.88 V (with only 350 mV loss, close to the thermodynamic limit) but time-resolved optical pump THz probe spectroscopy measurements estimated the charge-diffusion length for $\text{CH}_3\text{NH}_3\text{SnI}_3$ as only 30 nm, limiting overall device efficiencies.⁴⁵ However, the poor long-term stability and low reproducibility of these films

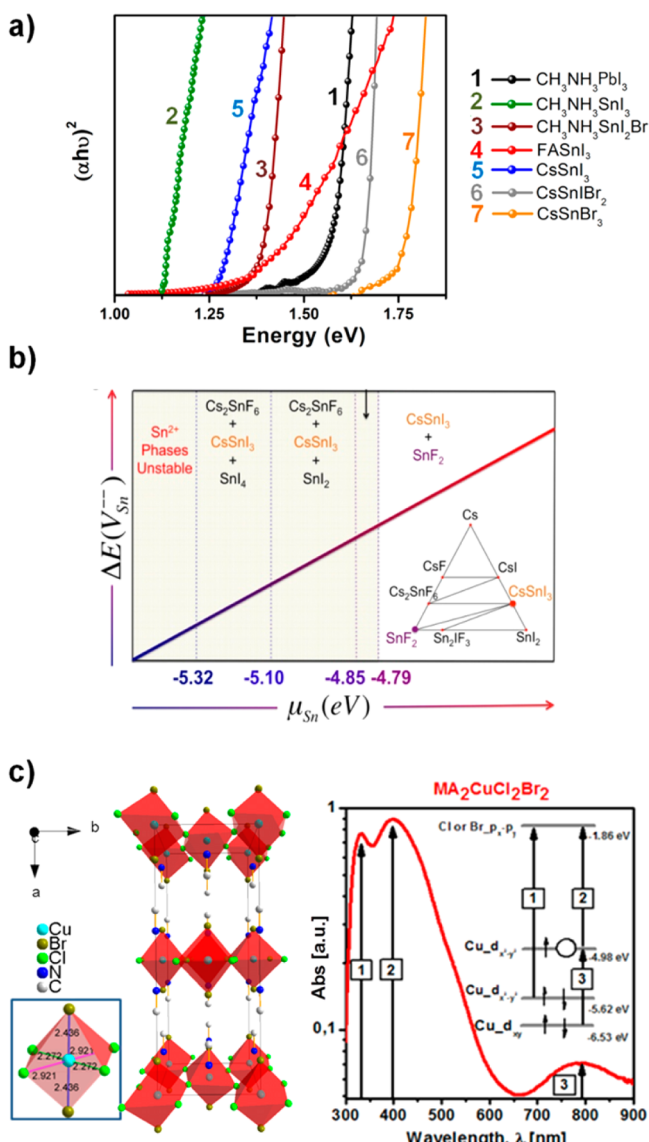


Figure 3. (a) Tauc plots of several lead-free perovskites films compared with $\text{CH}_3\text{NH}_3\text{PbI}_3$ one. (b) Calculated substitution in the Sn vacancy formation energy [$\Delta E(V_{\text{Sn}})$] at fixed Fermi level, as a function of the Sn chemical potential (μ_{Sn}). Reprinted from ref 47. (c) Crystal structure of $\text{MA}_2\text{CuCl}_2\text{Br}_2$, showing the alternation of organic and inorganic layers and absorption measured for $\text{MA}_2\text{CuCl}_2\text{Br}_2$. Inset: schematic representation of the electronic transitions 1 and 2 ($\text{Cu}_{\text{d}}_{x^2-y^2} \rightarrow \text{Cl}_{\text{p}_x-\text{p}_y}$) and d-d transitions 3 ($\text{Cu}_{\text{d}}_{xy} \rightarrow \text{Cu}_{\text{d}}_{x^2-y^2}$). Reprinted from ref 50.

caused by the tendency for Sn to get oxidized requires a careful re-evaluation of the $\text{CH}_3\text{NH}_3\text{SnI}_3$ system. Limited suppression of the Sn^{4+} formation and bulk recombination was tackled by SnF_2 addition in a report substituting Cs^+ ion for the CH_3NH_3^+ counterpart.⁴⁷ CsSnI_3 , an all inorganic Sn based perovskite is a p-type semiconductor with a band gap of 1.3 eV, previously used as hole transporting material for solid-state dye-sensitized solar cells.⁴⁸ The addition of SnF_2 to the low temperature perovskite solution process effectively reduced the background charge carrier density (holes) in the system (Figure 3b), improving the efficiency of the resulting device. However, like $\text{CH}_3\text{NH}_3\text{SnI}_3$, CsSnI_3 is also highly unstable in the ambient and the entire device was fabricated and tested inside the glovebox. Bromine doping/substitution to form $\text{CsSnI}_{3-x}\text{Br}_x$ ($0 \leq x \leq 3$) facilitate the tuning of the band gap and carrier concentration thus reducing recombination. The high open circuit voltages derived by the widening of the band gap by Br doping/substitution is translated in terms of depreciating carrier concentration and increased resistance to charge recombination,⁴⁹ but a clear improvement on the stability remains an objective.

The tendency for Sn to get oxidized requires a careful re-evaluation of the $\text{CH}_3\text{NH}_3\text{SnI}_3$ system.

Another candidate, germanium (Ge^{2+}) perovskites of the form CsGeX_3 ($X = \text{Cl}^-$, Br^- , I^-) with rhombohedral structure and $R\bar{3}m$ symmetry, are known for their nonlinear optical properties^{51,52} and have recently seen successful implementation as photovoltaic absorbers.⁵³ The maximum efficiency reported (3.2%, with $J_{\text{sc}} = 10.5 \text{ mA cm}^{-2}$ and $V_{\text{oc}} = 0.57 \text{ V}$) is still far below the performance of $\text{CH}_3\text{NH}_3\text{PbI}_3$, but with band gaps similar to their Pb counterparts (~1.6, ~2.3, and ~3.1 eV for I^- , Br^- , and Cl^- , respectively) suggest good prospects for these materials. Another variation of the Ge-perovskites, the orthorhombic $(\text{C}_4\text{H}_9\text{NH}_3)_2\text{GeI}_4$, shows a photoluminescence signal at 690 nm which suggests a suitable band gap.⁵⁴ As in most Pb-free perovskites reported thus far, the oxidation of the metal is a significant drawback; one that is arguably common to transition metal candidates, thus necessitating robust chemical stabilization technique for any successful implementation.

Transition metals such as Cu, Mn, Fe, Co, and Ni are promising alternatives to Sn and Pb, owing to their rich chemistries and multiple oxidation states. Transition metals with smaller ionic radii lead to steric hindrance to the 3D structure and trigger the formation of a layered configuration (Figure 3c), which is isostructural to compounds of the Ruddlesden–Popper phase (e.g., K_2NiF_4).⁵⁵ Such a layered structure was recently reported in the $(\text{CH}_3\text{NH}_3)_2\text{CuCl}_{4-x}\text{Br}_x$ series, where the presence of Cl was seen to be essential for stabilization against Cu^{2+} reduction.⁵⁰ The optical absorption is dominated by metal to ligand charge transfer transitions (Figure 3c) and their associated band gap can be tuned increasing the Br content from 2.48 eV (500 nm) for $(\text{CH}_3\text{NH}_3)_2\text{CuCl}_4$ to 1.80 eV (689 nm) for $(\text{CH}_3\text{NH}_3)_2\text{CuCl}_{0.5}\text{Br}_{3.5}$. An additional contribution to the absorption in the region between 700 and 900 nm comes from d–d transitions. Solar cells could be realized with infiltration of mesoporous titania with 2D copper perovskites, albeit with efficiencies lower than 0.02%. The partial copper reduction

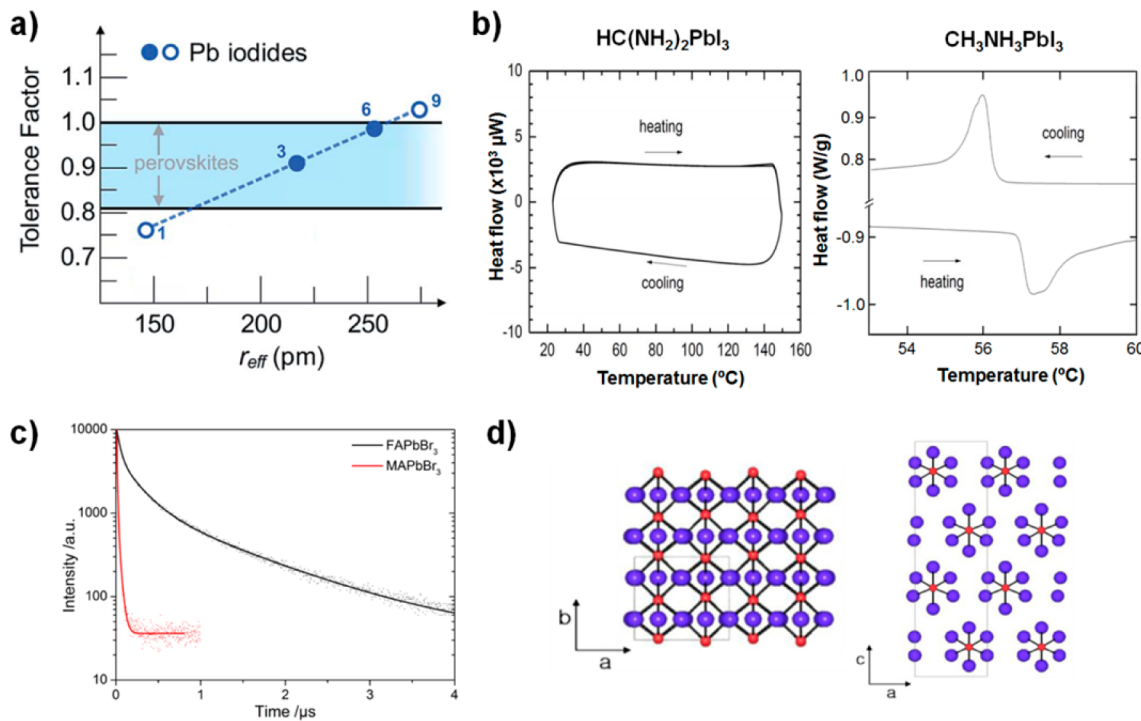


Figure 4. (a) Tolerance factors of Pb iodides plotted versus cation size. The numbers 1, 3, 6, and 9 represent NH_3^+ , CH_3NH_3^+ , $\text{HC}(\text{NH}_2)_2^+$, and $\text{CH}_3\text{CH}_2\text{NH}_3^+$, respectively. Open symbols indicate reported compounds with a nonperovskite structure. The light blue area highlights the range where perovskite-like frameworks are expected to form. The uncertainty in the tolerance factors is estimated to be 6%. Reproduced and modified from ref 63. (b) Differential scanning calorimetry (DSC) of $\text{HC}(\text{NH}_2)_2\text{PbI}_3$ showing no phase transition upon heating and cooling cycles, and of $\text{CH}_3\text{NH}_3\text{PbI}_3$ showing the phase transition from tetragonal to cubic. Reprinted from refs 64 and 16. (c) Comparison of the photoluminescence decay of FAPbBr_3 and MAPbBr_3 . Reprinted from ref 65. (d) Schematic crystal structure of $(\text{CH}_3\text{CH}_2\text{NH}_3)\text{PbI}_3$ where the red and purple spheres represent Pb and I ions, respectively. Reprinted from ref 66.

caused by bromine is responsible for the introduction of anion vacancies, which can act as electron traps, strongly limiting the cell efficiency. Charge injection at the contacts and into TiO_2 interface, transverse charge transport in the layered structure are also seen as challenges specifically to 2D materials and are detailed in subsequent sections.

Similar challenges derived from the lower dimensionality would be expected for the iron (Fe) perovskites. These 2D materials, with a tetragonal unit cell, present a general formula $(\text{RNH}_3)_2\text{FeX}_4$ with R = CH_3 , C_2H_5 , C_3H_7 , and $\text{C}_2\text{H}_5\text{CH}_2$ and where X = Cl, Br.^{56,57} As in the case of Sn, Ge the oxidation of the metal (Fe^{2+} to Fe^{3+}) is a source of instability. Though several studies have been performed on its magnetic properties,^{56–58} there is a lack of information regarding the optical or electrical properties; nevertheless, the yellow appearance reported suggests a band gap larger than the Pb perovskites.

Organic Cation Substitution. The monovalent cation in AMX_3 is a key component of the perovskite that determines its structure and dimensionality and has a direct impact on the stability and optoelectronic properties of the material. The cubooctahedral cavity, defined by the four edge-sharing MX_6 octahedra, permits the incorporation of only small cations into the 3D perovskite structure. The phenomenologically derived Goldschmidt tolerance factor⁵⁹ (t) allows an estimation of the stability of the perovskite based on the size of its constituents (Figure 4a). To obtain cubic phase, t should be 1; however, for most of the cubic perovskite structures the tolerance factor ranges from 0.78 to 1.05 due to a slight expansion in distorted structures.⁶⁰ To date, the most studied organic cation counterpart for replacing methylammonium (CH_3NH_3^+) has been formamidi-

num ($\text{HC}(\text{NH}_2)_2^+$), with a tolerance factor of 0.99, higher than $t = 0.91$ for $\text{CH}_3\text{NH}_3\text{PbI}_3$ (ion size: $\text{HC}(\text{NH}_2)_2^+$, 2.53 Å; CH_3NH_3^+ , 2.17 Å; Pb^{2+} , 1.19 Å; and I^- , 2.20 Å).

The perovskite crystal lattice expands as the size of cation increases (ionic radii $\text{Cs} < \text{CH}_3\text{NH}_3 < \text{HC}(\text{NH}_2)_2^+$), leading to smaller band gap, as evidenced in CsPbI_3 , $\text{CH}_3\text{NH}_3\text{PbI}_3$, and $\text{HC}(\text{NH}_2)_2\text{PbI}_3$ ⁶¹ (1.73, 1.57, and 1.48 eV, respectively; Table 1). However, when the metal center is replaced by a smaller

Table 1. Relationship between Band Gap and the Cationic Radius in APbI_3 and ASnI_3 Perovskite System

	Cs^+	CH_3NH_3^+	$\text{HC}(\text{NH}_2)_2^+$
band gap (APbI_3)	1.73	1.55	1.47
band gap (ASnI_3)	1.30	1.20	1.41
difference in band gap (eV)	0.43	0.35	0.06
ionic radii (Å)	1.81	2.70	2.79

Sn^{2+} metal ion, the relationship between cation size and its band gap is altered. For example, the variation in band gap of CsPbI_3 and CsSnI_3 is larger (~0.43 eV) compared to that between $\text{HC}(\text{NH}_2)_2\text{PbI}_3$ and $\text{HC}(\text{NH}_2)_2\text{SnI}_3$ (~0.06 eV). Replacement of cations also alters other intrinsic properties of the perovskite, including its stability; for instance, CsPbI_3 has been shown to be unstable and tends to transform into Cs_4PbI_6 .⁶²

Although, the band gap is reduced from 1.55 to 1.48 eV⁶⁷ by replacing the methylammonium with formamidinium cation, the first attempt of using $\text{HC}(\text{NH}_2)_2\text{PbI}_3$ as light absorber resulted in a power conversion efficiency of only 4.3%²⁰ due to the presence of a yellow polymorph with a nonperovskite

structure. Subsequent reports⁶⁴ boosted the efficiency of $\text{HC}(\text{NH}_2)_2\text{PbI}_3$ to over 14% by increasing the annealing temperature and enhancing the formation of the black perovskite polymorph. The efficiency of $\text{HC}(\text{NH}_2)_2\text{PbI}_3$ solar cells was further enhanced to 16.01% by improving the charge collection with an extra thin layer of $\text{CH}_3\text{NH}_3\text{PbI}_3$ perovskite on top, thus enabling better light absorption above 700 nm. In addition to the high efficiency, $\text{HC}(\text{NH}_2)_2\text{PbI}_3$ does not display a phase transition at 57 °C (Figure 4b), which represents a thermal stability advantage compared to $\text{CH}_3\text{NH}_3\text{PbI}_3$.⁶⁴ A mixed cation perovskite can be formed by a partial substitution of the CH_3NH_3^+ . Using a sequential deposition method, PbI_2 was reacted with a MAI/ $\text{HC}(\text{NH}_2)_2\text{I}$ mixture. The improved power conversion efficiency (14.9%) of $(\text{CH}_3\text{NH}_3)_{0.6}(\text{HC}(\text{NH}_2)_2)_{0.4}\text{PbI}_3$ was attributed to better light harvesting and collection efficiency in this mixed-cation lead iodide perovskite material.⁶⁸

In the lead-bromide perovskites,⁶⁵ planar devices based on $\text{HC}(\text{NH}_2)_2$ and CH_3NH_3 showed that $\text{HC}(\text{NH}_2)_2\text{PbBr}_3$ exhibited longer PL lifetimes and larger charge diffusion length compared to $\text{CH}_3\text{NH}_3\text{PbBr}_3$ (~200 ns vs ~17 ns, Figure 4c). Although the reason for the superior charge diffusion length in FAPbBr_3 warrants further study, the findings suggest that intrinsic electronic properties of 3D perovskite may be supplemented by replacing methylammonium with other cations. Candidates such as ethylammonium, $(\text{CH}_3\text{CH}_2\text{NH}_3)^+$, have been used in 2H perovskites for photovoltaic applications⁶⁶ (Figure 4d), though it was with power conversion efficiency much lower than those for methylammonium and formamidinium based perovskites. In the search of new alternatives, the Goldschmidt tolerance factor should be taken into consideration for exploring other cations. Several options⁶⁹ to be considered include hydroxylammonium $[\text{H}_3\text{NOH}]^+$, hydrazinium $[\text{H}_3\text{N}-\text{NH}_2]^+$, azetidinium $[(\text{CH}_2)_3\text{NH}_2]^+$, imidazolium $[\text{C}_3\text{N}_2\text{H}_5]^+$ and guanidinium $[\text{C}(\text{NH}_2)_3]^+$.⁶³ Their promising estimated tolerance factors offer the possibility of forming a cubical 3D perovskite, with the subsequent advantageous electrical and optical properties. However, their applications in photovoltaics are yet to be reported.

Multidimensional Perovskites. In the 3D perovskite, the anionic MX_6 octahedra are condensed into three-dimensional network; however, the size of the cation plays a critical role in determining the thickness and separation of the inorganic layers: if the cation size is too large, it cannot fit into the rigid 3D perovskite network and, thus, separates the system into layers, forming lower dimensional networks (2D, Figure 5a). With a general formula of $(\text{R}-\text{NH}_3)_2\text{MX}_4$, where $\text{R}-\text{NH}_3^+$ is an aliphatic or single ring aromatic cation,⁷⁰ the 2D perovskites can have two orientations, $\langle 110 \rangle$ or $\langle 100 \rangle$. They can form single or bilayer intercalated organic molecules for monoammonium ($\text{R}-\text{NH}_3^+$) or diammonium ($^+\text{NH}_3-\text{R}-\text{NH}_3^+$) cation respectively (Figure 5a). Generally, these lower dimensional perovskites possess higher exciton binding energies and poor conductivity in certain crystallographic directions,⁵⁵ along with significantly higher band gap compared to the 3D perovskites.⁷¹ These properties have led them to be exploited for light emission applications,^{72,73} but 2D perovskites have more flexible structures, with more relaxed limitations in the size of the organic cations. Therefore, this offers the opportunity of tuning of the photophysical and electronic properties, opening new opportunities for photovoltaic applications.

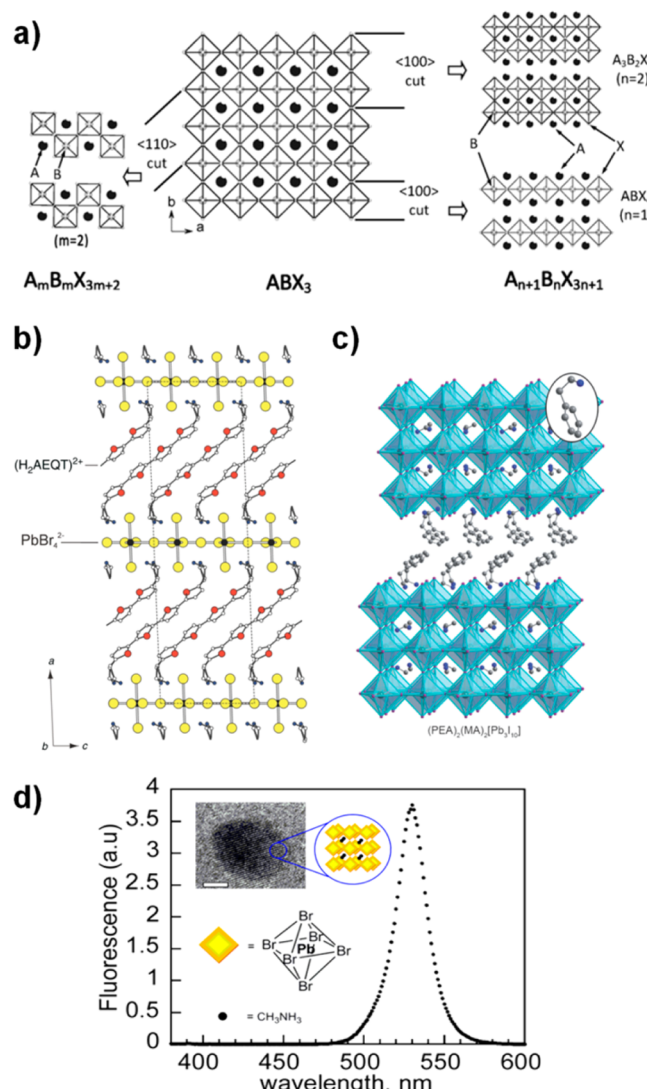


Figure 5. (a) Schematic representation of 2D perovskites based on $\langle 100 \rangle$, $n = 1, 2$ (right) and $\langle 110 \rangle$, $m = 2$ (left) networks, obtained from cuts of the parent ABX_3 structure. Reprinted from ref 80. (b) Crystal structure of $(\text{H}_2\text{AEQT})\text{PbBr}_4$, viewed down the b axis. Reprinted from ref 21. (c) 2D perovskite $(\text{PEA})_2(\text{MA})_2[\text{Pb}_3\text{I}_{10}]$. Inset: a PEA cation in the organic layers. Atom colors: Pb = turquoise; I = purple; N = blue; C = gray. Disordered atoms and hydrogens omitted for clarity. Reproduced from ref 81. (d) Photoluminescence of POA_2 , where OA refers to octylammonium cation and 2 indicates the ratio of $\text{CH}_3(\text{CH}_2)_7\text{NH}_3\text{Br}/\text{CH}_3\text{NH}_3\text{Br} = 0.6:0.4$. Inset shows the HRTEM image of an isolated perovskite nanoparticle (scale bar 2 nm) and schematic representation of an array of corner sharing MX_6 octahedra confined in the three dimensions due to the organic capping. Reproduced from ref 82.

The strategies to design suitable 2D perovskites for photovoltaic applications include enhancing hydrogen or halogen bonding between organic cation and inorganic framework to reduce the band gap.^{74–76} Similarly, the exciton binding energy has also been shown to decrease with increasing inorganic layer (indicated by n , see Figure 2d).^{71,77} However, the key factor that would have to be addressed when implementing multidimensional perovskites is the improvement in charge transport. The charge carrier mobility in 2D perovskite can possibly be improved by connecting the inorganic layers by covalent bridges,⁷⁸ which allows an

enhancement in the conductivity of the nonpreferred orientations, thus increasing the diffusion lengths in these materials. Infiltrating these 2D perovskites within a mesoporous scaffold could also improve the charge transport within solar cells. Additionally cations with the appropriate molecular energy levels can improve the charge transfer between and the separated inorganic layers. An example of this is the AEQT²⁺ sandwiched lead(II) halide perovskite (Figure 5b), in which each quaterthiophene is ordered in a herringbone arrangement with respect to the adjacent quaterthiophene.⁷⁹

Tuning low dimensional perovskites can also have implications on critical issues as moisture stability. In this direction, the recent use of a 2D perovskite, $(\text{PEA})_2(\text{MA})_2[\text{Pb}_3\text{I}_{10}]$, (with $\text{PEA}=\text{C}_6\text{H}_5(\text{CH}_2)_2\text{NH}_3^+$ and $\text{MA}=\text{CH}_3\text{NH}_3^+$, Figure 5c) as a photovoltaic absorber has yielded power conversion efficiencies close to 5%.⁸¹ By controlling the stoichiometric amount of organic cations and lead iodide precursors, a layered perovskite structure (with $n=3$) is formed through a self-assembly process. The structural modification which also resulted in much more planar films increased the air stability compared to its 3D analogue. However, the device performance for the 2D perovskite is limited by poor charge extraction. Thus, proper material/device architectural design for better charge collection is extremely important for improving the photovoltaic performance of 2D perovskites.

Low dimensional perovskites can also have implications on critical issues as moisture stability.

Utilization of still longer organic chains entirely disrupts the 3D connectivity and produces yet another interesting variant (Figure 5d). Using ammonium bromide as capping ligands, 6-nm-size nanoparticles of $\text{CH}_3\text{NH}_3\text{PbBr}_3$ were successfully synthesized and dispersed in organic solvents, thus making them amenable to thin film formation by spin-coating.⁸³ Both the colloidal solution and thin films display remarkably high fluorescent quantum efficiency and narrow emission band. As in higher dimensionality perovskites, the luminescent properties of these nanoparticles can be modulated by changing either the methylammonium cation or the capping organic chain. Because the capping layer of the perovskite nanoparticles and the discontinuous structure hinders the electrical conductivity, the possible use of these nanoparticles for photovoltaic applications would benefit from a sensitization approach analogous to quantum dot solar cells, where the photo-generated charge is directly injected into the electron and hole transporting materials.

Prospects. The use of lead-halide perovskites has represented a breakthrough in the photovoltaic field; nevertheless, with major deficiencies of instability and toxicity. The rich diversity these compounds offer are making it imperative to revisit literature in these fields and evaluate the photovoltaic properties of materials as diverse as organometallics, inorganic multi-component halides and perovskite oxides among others. Early gains in device architecture, process engineering, and halide substitutions have yielded phenomenal success with efficiencies above 20%. However, further improvements in conversion efficiencies will be more difficult to realize. The breakthrough possibility will come from new materials concepts that may include nonperovskite variants of existing materials' families,

perovskite families that are yet to be explored for photovoltaics, judicious design of interfaces,¹⁵ and alternative device architectures that could include perovskite-thin film tandem cells.⁸³

An example of such a new material set is Cs_2SnI_6 (Sn in the Sn^{4+} state, band gap of 1.26 eV) which is an air-stable iodosalt with a nonperovskite structure.⁸⁴ If made semiconducting, it would function well as an excellent air-stable absorber. Another future direction would involve the rational design of photoferroelectrics, as has been observed in oxide perovskites. One such oxide that has made the successful transition to solar cell applications is multiferroic $\text{Bi}_2\text{FeCrO}_6$. This epitaxially grown material achieved power conversion efficiencies above 8% in multilayered thin film solar cells.⁸⁵ Combining photoresponse and polarization-induced charge-separation is a fundamentally different mechanism compared to conventional semiconductor solar cells.⁸⁶ This possibility of facile separation of photo-induced charge carriers under an electric field higher than the built-in voltage of conventional p–n junctions holds the promise of challenging the theoretical limits of perovskite solar cells, reported to be up to 30%.⁴⁰

The principal success of $\text{CH}_3\text{NH}_3\text{PbI}_3$ has been attributed to the Pb lone-pair 6s orbitals and the Pm3m yielding excellent absorption, small effective charge carrier masses, dominant point defects that only generate shallow levels, and benign grain boundaries.⁴⁰ Such a structure–property-function nexus seems to be elusive in the quest to replace Pb with materials such as Cu, Fe, Mn, Co, and Ni. The most promising way forward arguably is to employ these materials in multifunctional perovskite formulations that allow for apt band gaps and unimpeded carrier mobility facilitated by the inorganics, with the organic moieties providing additional controls for stability, light harvesting, and intralayer charge transport. The prospects for advancing photoconversion efficiencies and manufacturability are contingent upon addressing the unavoidable issues of toxicity and stability through rational design and synthesis leveraging on the versatility of halide perovskite family. Newer semiconducting halide materials are necessary for perovskite solar cells to make the transition from laboratory curiosity to a practical photovoltaic technology. This quest for materials innovation to deliver green, ultrahigh performance stable optical absorbers promises to write the next chapter in this extraordinary ascension of perovskite solar cells.

■ AUTHOR INFORMATION

Corresponding Authors

*E-mail: PBPablo@ntu.edu.sg

*E-mail: Subodh@ntu.edu.sg

Notes

The authors declare no competing financial interest.

Biographies

Pablo P. Boix received his Ph.D. from the Universitat Jaume I (2012, Castelló, Spain). During this period, he analyzed the physical processes of optoelectrical devices including DSC, QDSC, organic photovoltaics, and water splitting systems by impedance spectroscopy. In 2012, he joined ERI@N, where his research focuses on the development of perovskite solar cells, unveiling the working mechanisms which determine the performance of these photoelectrical devices.

Shweta Agarwala obtained her Ph.D. in electronics engineering in 2011 from National University of Singapore (NUS) on nanostructured materials for dye-sensitized solar cells. Currently, she is a research fellow at ERI@N, NTU. Her research is aimed at new synthesis

pathways for porous inorganic nanomaterials and perovskite materials for solar energy applications.

Teck Ming is pursuing his Ph.D. in Materials Science and Engineering at Nanyang Technological University (NTU). He started his studies on cobalt-based liquid electrolytes for dye-sensitized solar cells. Currently, he works on perovskite-based solid-state solar cells under the supervision of Prof. Subodh in the Energy Research Institute @ NTU.

Nripan Mathews is an Assistant Professor at the School of Materials Science and Engineering and the Energy Research Institute at Nanyang Technological University. His primary research interests are photovoltaics, field effect transistors, and photoelectrochemical systems.

Subodh G. Mhaisalkar is Tan Chin Tuan Centennial Professor in the School of Materials Science & Engineering at the Nanyang Technological University, Singapore, and currently heads the Energy Research Initiative @ NTU (ERI@N). His main areas of research comprise perovskite solar cells, printed electronics, and energy storage. Subodh received his Bachelors' degree from IIT-Bombay and his M.S. and Ph.D. degrees from The Ohio State University.

ACKNOWLEDGMENTS

Financial support from NTU start-up grant M4081293, Singapore NRF through the Competitive Research Program (NRF-CRP4-2008-03) and the Singapore–Berkeley Research Initiative for Sustainable Energy (SinBeRISE) CREATE Programme is gratefully acknowledged.

REFERENCES

- (1) Nuraje, N.; Su, K. Perovskite Ferroelectric Nanomaterials. *Nanoscale* **2013**, *5*, 8752–80.
- (2) Mitzi, D. B.; Watson, I. B. M. T. J.; Box, I. *Prog. Inorg. Chem.*; John Wiley & Sons, Inc.: Hoboken, NJ, 1999; Vol. 48.
- (3) NREL. http://www.nrel.gov/ncpv/images/efficiency_chart.jpg (accessed Jan 2015).
- (4) De Wolf, S.; Holovsky, J.; Moon, S.-J.; Löper, P.; Niesen, B.; Ledinsky, M.; Haug, F.-J.; Yum, J.-H.; Ballif, C. Organometallic Halide Perovskites: Sharp Optical Absorption Edge and Its Relation to Photovoltaic Performance. *J. Phys. Chem. Lett.* **2014**, *5*, 1035–1039.
- (5) D'Innocenzo, V.; Grancini, G.; Alcocer, M. J. P.; Kandada, A. R. S.; Stranks, S. D.; Lee, M. M.; Lanzani, G.; Snaith, H. J.; Petrozza, A. Excitons Versus Free Charges In Organo-Lead Tri-Halide Perovskites. *Nat. Commun.* **2014**, *5*, 3586–3586.
- (6) Manser, J. S.; Kamat, P. V. Band Filling With Free Charge Carriers In Organometal Halide Perovskites. *Nat. Photonics* **2014**, *8*, 737–743.
- (7) Xing, G.; Mathews, N.; Sun, S.; Lim, S. S.; Lam, Y. M.; Gratzel, M.; Mhaisalkar, S.; Sum, T. C. Long-Range Balanced Electron- and Hole-Transport Lengths in Organic–Inorganic $\text{CH}_3\text{NH}_3\text{PbI}_3$. *Science* **2013**, *342*, 344–347.
- (8) Stranks, S. D.; Eperon, G. E.; Grancini, G.; Menelaou, C.; Alcocer, M. J. P.; Leijtens, T.; Herz, L. M.; Petrozza, a.; Snaith, H. J. Electron-Hole Diffusion Lengths Exceeding 1 Micrometer in an Organometal Trihalide Perovskite Absorber. *Science* **2013**, *342*, 341–344.
- (9) Wei, Z.; Chen, H.; Yan, K.; Yang, S. Inkjet Printing and Instant Chemical Transformation of a $\text{CH}_3\text{NH}_3\text{PbI}_3$ /Nanocarbon Electrode and Interface for Planar Perovskite Solar Cells. *Angew. Chem.* **2014**, *126*, 13455–13459.
- (10) Li, Z.; Kulkarni, S. a.; Boix, P. P.; Shi, E.; Cao, A.; Fu, K.; Batabyal, S. K.; Zhang, J.; Xiong, Q.; Wong, et al. Laminated Carbon Nanotube Networks For Metal Electrode-Free Efficient Perovskite Solar Cells. *ACS Nano* **2014**, *8*, 6797–804.
- (11) Qin, P.; Tanaka, S.; Ito, S.; Tetraeault, N.; Manabe, K.; Nishino, H.; Nazeeruddin, M. K.; Grätzel, M. Inorganic Hole Conductor-Based Lead Halide Perovskite Solar Cells With 12.4% Conversion Efficiency. *Nat. Commun.* **2014**, *5*, 3834–3834.
- (12) Burschka, J.; Pellet, N.; Moon, S.-J.; Humphry-Baker, R.; Gao, P.; Nazeeruddin, M. K.; Grätzel, M. Sequential Deposition As A Route To High-Performance Perovskite-Sensitized Solar Cells. *Nature* **2013**, *499*, 316–9.
- (13) Xiao, M.; Huang, F.; Huang, W.; Dkhissi, Y.; Zhu, Y.; Etheridge, J.; Gray-Weale, A.; Bach, U.; Cheng, Y. B.; Spiccia, L. A Fast Deposition-Crystallization Procedure For Highly Efficient Lead Iodide Perovskite Thin-Film Solar Cells. *Angew. Chem., Int. Ed. Engl.* **2014**, *53*, 9898–903.
- (14) Liu, M.; Johnston, M. B.; Snaith, H. J. Efficient Planar Heterojunction Perovskite Solar Cells By Vapour Deposition. *Nature* **2013**, *501*, 395–8.
- (15) Zhou, H.; Chen, Q.; Li, G.; Luo, S.; Song, T. b.; Duan, H. S.; Hong, Z.; You, J.; Liu, Y.; Yang, Y. Interface Engineering Of Highly Efficient Perovskite Solar Cells. *Science* **2014**, *345*, 542–546.
- (16) Baikie, T.; Fang, Y.; Kadro, J. M.; Schreyer, M. K.; Wei, F.; Mhaisalkar, S. G.; Grätzel, M.; White, T. Synthesis and Crystal Chemistry of the Hybrid Perovskite $(\text{CH}_3\text{NH}_3)\text{PbI}_3$ for Solid State Sensitised Solar Cell Applications. *J. Mater. Chem. A* **2013**, *1*, 5628–5641.
- (17) Green, M.; Ho-Baillie, A.; Snaith, H. J. The Emergence of Perovskite Solar Cells. *Nat. Photonics* **2014**, *8*, 506–514.
- (18) Schulz, P.; Edri, E.; Kirmayer, S.; Hodes, G.; Cahen, D.; Kahn, A. Interface Energetics in Organo-Metal Halide Perovskite-based Photovoltaic Cells. *Energy Environ. Sci.* **2014**, *7*, 1377–1381.
- (19) Ogomi, Y.; Morita, A.; Tsukamoto, S.; Saitho, T.; Fujikawa, N.; Shen, Q.; Toyoda, T.; Yoshino, K.; Pandey, S. S.; Ma, T.; et al. $\text{CH}_3\text{NH}_3\text{Sn}_x\text{Pb}_{(1-x)}\text{I}_3$ Perovskite Solar Cells Covering up to 1060 nm. *J. Phys. Chem. Lett.* **2014**, *5*, 1004–1011.
- (20) Koh, T. M.; Fu, K.; Fang, Y.; Chen, S.; Sum, T. C.; Mathews, N.; Mhaisalkar, S. G.; Boix, P. P.; Baikie, T. Formamidinium-Containing Metal-Halide: An Alternative Material for Near-IR Absorption Perovskite Solar Cells. *J. Phys. Chem. C* **2013**, *118*, 16458–16462.
- (21) Mitzi, D. B. Templating And Structural Engineering In Organic–Inorganic Perovskites. *J. Chem. Soc., Dalton Trans.* **2001**, *1*, 1–12.
- (22) Kojima, A.; Teshima, K.; Shirai, Y.; Miyasaka, T. Organometal Halide Perovskites As Visible-Light Sensitzers For Photovoltaic Cells. *J. Am. Chem. Soc.* **2009**, *131*, 6050–1.
- (23) Tanaka, K.; Takahashi, T.; Ban, T.; Kondo, T.; Uchida, K.; Miura, N. Comparative Study On The Excitons In Lead-Halide-Based Perovskite-Type Crystals $\text{CH}_3\text{NH}_3\text{PbBr}_3$ $\text{CH}_3\text{NH}_3\text{PbI}_3$. *Solid State Commun.* **2003**, *127*, 619–623.
- (24) Edri, E.; Kirmayer, S.; Cahen, D.; Hodes, G. High Open-Circuit Voltage Solar Cells Based on Organic–Inorganic Lead Bromide Perovskite. *J. Phys. Chem. Lett.* **2013**, *4*, 897–902.
- (25) Edri, E.; Kirmayer, S.; Kulbak, M.; Hodes, G.; Cahen, D. Chloride Inclusion and Hole Transport Material Doping Improve Methyl Ammonium Lead Bromide Perovskite-based High Open-Circuit Voltage Solar Cells. *J. Phys. Chem. Lett.* **2014**, *5*, 429–433.
- (26) Cai, B.; Xing, Y.; Yang, Z.; Zhang, W.; Qiu, J. High Performance Hybrid Solar Cells Sensitized By Organolead Halide Perovskites. *Energy Environ. Sci.* **2013**, *6*, 1480–1480.
- (27) Kim, H.-s.; Mora-Sero, I.; Gonzalez-Pedro, V.; Fabregat-Santiago, F.; Juarez-Perez, E. J.; Park, N.-g.; Bisquert, J. Mechanism Of Carrier Accumulation In Perovskite Thin-Absorber Solar Cells. *Nat. Commun.* **2013**, *4*, 2242–2242.
- (28) Ryu, S.; Noh, J. H.; Jeon, N. J.; Kim, Y. C.; Yang, W. S.; Seo, J. W.; Seok, S. I. Voltage Output of Efficient Perovskite Solar Cells with high Open-Circuit Voltage and Fill Factor. *Energy Environ. Sci.* **2014**, *7*, 2614–2618.
- (29) Suarez, B.; Gonzalez-Pedro, V.; Ripolles, T. S.; Sanchez, R. S.; Otero, L.; Mora-Sero, I. Recombination Study of Combined Halides (Cl , Br , I) Perovskite Solar Cells. *J. Phys. Chem. Lett.* **2014**, *5*, 1628–1635.

- (30) Kulkarni, S. A.; Baikie, T.; Boix, P. P.; Yantara, N.; Mathews, N.; Mhaisalkar, S. Band-Gap Tuning Of Lead Halide Perovskites Using A Sequential Deposition Process. *J. Mater. Chem. A* **2014**, *2*, 9221–9221.
- (31) Heo, J. H.; Song, D. H.; Im, S. H. Planar $\text{CH}_3\text{NH}_3\text{PbBr}_3$ Hybrid Solar Cells with 10.4% Power Conversion Efficiency, Fabricated by Controlled Crystallization in the Spin-Coating Process. *Adv. Mater.* **2014**, *26*, 8179–8183.
- (32) Ball, J. M.; Lee, M. M.; Hey, A.; Snaith, H. Low-Temperature Processed Mesosuperstructured to Thin-Film Perovskite Solar Cells. *Energy Environ. Sci.* **2013**, *6*, 1739–1743.
- (33) Colella, S.; Mosconi, E.; Fedeli, P.; Listorti, A.; Gazza, F.; Orlandi, F.; Ferro, P.; Besagni, T.; Rizzo, A.; Calestani, G.; Gigli, G.; De Angelis, F.; Mosca, R. $\text{MAPbI}_{3-x}\text{Cl}_x$ Mixed Halide Perovskite for Hybrid Solar Cells: The Role of Chloride as Dopant on the Transport and Structural Properties. *Chem. Mater.* **2013**, *25*, 4613–4618.
- (34) Docampo, P.; Hanusch, F.; Stranks, S. D.; Döblinger, M.; Feckl, J. M.; Ehrenspurger, M.; Minar, N. K.; Johnston, M. B.; Snaith, H. J.; Bein, T. Solution Deposition-Conversion for Planar Heterojunction Mixed Halide Perovskite Solar Cells. *Adv. Energy Mater.* **2014**, *4*.
- (35) Sabba, D.; Dewi, H. A.; Prabhakar, R. R.; Baikie, T.; Chen, S.; Du, Y.; Mathews, N.; Boix, P. P.; Mhaisalkar, S. G. Incorporation Of Cl In Sequentially Deposited Lead Halide Perovskite Films For Highly Efficient Mesoporous Solar Cells. *Nanoscale* **2014**, *6*, 13854–13860.
- (36) Tidhar, Y.; Edri, E.; Weissman, H.; Zohar, D.; Hodes, G.; Cahen, D.; Rybtchinski, B.; Kirmayer, S. Crystallization of Methyl Ammonium Lead Halide Perovskites: Implications for Photovoltaic Applications. *J. Am. Chem. Soc.* **2014**, *136*, 13249–13256.
- (37) Jeon, N. J.; Noh, J. H.; Kim, Y. C.; Yang, W. S.; Ryu, S.; Seok, S. I. Solvent Engineering For High-Performance Inorganic–Organic Hybrid Perovskite Solar Cells. *Nat. Mater.* **2014**, *13*, 897–903.
- (38) Poglitsch, A.; Weber, D. Dynamic Disorder In Methylammoniumtrihalogenoplumbates (II) Observed By Millimeter-Wave Spectroscopy. *J. Chem. Phys.* **1987**, *87*, 6373–6373.
- (39) Maalej, A.; Abid, Y.; Kallel, A.; Daoud, A.; Lautié, A.; Romain, F. Phase Transitions And Crystal Dynamics In The Cubic Perovskite $\text{CH}_3\text{NH}_3\text{PbCl}_3$. *Solid State Commun.* **1997**, *103*, 279–284.
- (40) Yin, W.-J.; Shi, T.; Yan, Y. Unique Properties of Halide Perovskites as Possible Origins of the Superior Solar Cell Performance. *Adv. Mater.* **2014**, *1*–6.
- (41) Mitzi, D. B.; Feild, C. A.; Harrison, W. T. A. Conducting Tin Halides with a Layered Organic-Based Perovskite Structure. *Nature* **1994**, *369*, 467–469.
- (42) Hao, F.; Stoumpos, C. C.; Chang, R. P. H.; Kanatzidis, M. G. Anomalous Band Gap Behavior In Mixed Sn And Pb Perovskites Enables Broadening Of Absorption Spectrum In Solar Cells. *J. Am. Chem. Soc.* **2014**, *136*, 8094–8099.
- (43) Zuo, F.; Williams, S. T.; Liang, P. W.; Chueh, C. C.; Liao, C. Y.; Jen, A. K. Y. Binary-Metal Perovskites Toward High-Performance Planar-Heterojunction Hybrid Solar Cells. *Adv. Mater.* **2014**, *26*, 6454–6460.
- (44) Hao, F.; Stoumpos, C. C.; Cao, D. H.; Chang, R. P. H.; Kanatzidis, M. G. Lead-Free Solid-State Organic–Inorganic Halide Perovskite Solar Cells. *Nat. Photonics* **2014**, *8*, 489–494.
- (45) Noel, N. K.; Stranks, S. D.; Abate, A.; Wehrenfennig, C.; Guarnera, S.; Haghhighirad, A.; Sadhanala, A.; Eperon, G. E.; Pathak, S. K.; Johnston, M. B.; et al. Lead-Free Organic–Inorganic Tin Halide Perovskites For Photovoltaic Applications. *Energy Environ. Sci.* **2014**, *7*, 3061–3068.
- (46) Shockley, W.; Queisser, H. J. Detailed Balance Limit of Efficiency of p-n Junction Solar Cells. *J. Appl. Phys.* **1961**, *32*, 510–510.
- (47) Kumar, M. H.; Dharani, S.; Leong, W. L.; Boix, P. P.; Prabhakar, R. R.; Baikie, T.; Shi, C.; Ding, H.; Ramesh, R.; Asta, M.; et al. Lead-Free Halide Perovskite Solar Cells with High Photocurrents Realized Through Vacancy Modulation. *Adv. Mater.* **2014**, *26*, 7122–7127.
- (48) Chung, I.; Lee, B.; He, J.; Chang, R. P. H.; Kanatzidis, M. G. All-Solid-State Dye-Sensitized Solar Cells With High Efficiency. *Nature* **2012**, *485*, 486–489.
- (49) Sabba, D.; Mulmudi, H. K.; Prabhakar, R. R. Impact of Anionic Br-Substitution on Open Circuit Voltage in Lead Free Perovskite ($\text{CsSnI}_3\text{xBr}_x$) Solar Cells. *J. Phys. Chem. C* **2015**, *119*, 1763–1767.
- (50) Cortecchia, D.; Dewi, H. A.; Dharani, S.; Baikie, T.; Soci, C.; Mathews, N. “Green” 2D Hybrid Perovskites for Perovskite-Based Solar Cells. In *EOSAM 2014*, European Optical Society: Berlin, 2014.
- (51) Tang, L. C.; Chang, C. S.; Huang, J. Y. Electronic Structure And Optical Properties Of Rhombohedral CsGeI_3 Crystal. *J. Phys.: Condens. Matter* **2000**, *12*, 9129–9143.
- (52) Tang, L. C.; Huang, J. Y.; Chang, C. S.; Lee, M. H.; Liu, L. Q. New Infrared Nonlinear Optical Crystal CsGeBr_3 : Synthesis, Structure And Powder Second-Harmonic Generation Properties. *J. Phys.: Condens. Matter* **2005**, *17*, 7275–7286.
- (53) Huang, C.; Yan, X. C.; Cui, G.; Liu, Z.; Pang, S.; Xu, H. New Germanium-Containing Perovskite Materials And Their Application In Solar Cells. Chinese Pat. Appl. CN 201410173750, 2014, <http://www.google.com/patents/CN103943368A?cl=en>.
- (54) Mitzi, D. B. Synthesis, Crystal Structure, and Optical and Thermal Properties of $(\text{C}_4\text{H}_9\text{NH}_3)_2\text{MI}_4$ ($\text{M} = \text{Ge}, \text{Sn}, \text{Pb}$). *Chem. Mater.* **1996**, *8*, 791–800.
- (55) Cheng, Z.; Lin, J. Layered Organic–Inorganic Hybrid Perovskites: Structure, Optical Properties, Film Preparation, Patterning And Templating Engineering. *CrystEngComm* **2010**, *12*, 2646–2662.
- (56) Mostafa, M. F.; Semary, M. A.; Ahmed, M. A. Field Dependence Of The Susceptibility Maximum For Two-Dimensional Antiferromagnet. *Phys. Lett. A* **1977**, *61*, 183–184.
- (57) Mostafa, M. F.; Willett, R. D. Magnetic Properties of Ferrous Chloride Complexes with Two-Dimensional Structures. *Phys. Rev. B* **1971**, *4*, 2213–2215.
- (58) Semary, M. A.; Mostafa, M. F.; Ahmed, M. A. Magnetic Susceptibility Of $(\text{CH}_3\text{NH}_3)_2\text{FeCl}_3\text{Br}$: An Example Of A Canted Spin System. *Solid State Commun.* **1978**, *25*, 443–445.
- (59) Li, C.; Lu, X.; Ding, W.; Feng, L.; Gao, Y.; Guo, Z. Formability of ABX_3 ($\text{X} = \text{F}, \text{Cl}, \text{Br}, \text{I}$) halide perovskites. *Acta Crystallogr., Sect. B* **2008**, *64*, 702–707.
- (60) Randall, C. A.; Bhalla, A. S.; Shrout, T. R.; Cross, L. E. Classification And Consequences Of Complex Lead Perovskite Ferroelectrics With Regard To B-Site Cation Order. *J. Mater. Res.* **1990**, *5*, 829–834.
- (61) Eperon, G. E.; Stranks, S. D.; Menelaou, C.; Johnston, M. B.; Herz, L. M.; Snaith, H. J. Formamidinium Lead Trihalide: A Broadly Tunable Perovskite For Efficient Planar Heterojunction Solar Cells. *Energy Environ. Sci.* **2014**, *7*, 982–988.
- (62) Yunakova, O. N.; Miloslavskii, V. K.; Kovalenko, E. N. Exciton Absorption Spectrum of Thin CsPbI_3 and Cs_4PbI_6 Films. *Opt. Spectrosc.* **2012**, *112*, 91–96.
- (63) Gregor, K.; Shijing, S.; Anthony, K. C. Solid-State Principles Applied To Organic–Inorganic Perovskites: New Tricks For An Old Dog. *Chem. Sci.* **2014**, *5*, 4712–4715.
- (64) Lee, J.-W.; Seol, D.-J.; Cho, A.-N.; Park, N.-G. High-Efficiency Perovskite Solar Cells Based on the Black Polymorph of $\text{HC}(\text{NH}_2)_2\text{PbI}_3$. *Adv. Mater.* **2014**, *26*, 4991–4998.
- (65) Hanusch, F. C.; Wiesenmayer, E.; Mankel, E.; Binek, A.; Angloher, P.; Fraunhofer, C.; Giesbrecht, N.; Feckl, J. M.; Jaegermann, W.; Johrendt, D.; et al. Efficient Planar Heterojunction Perovskite Solar Cells Based on Formamidinium Lead Bromide. *J. Phys. Chem. Lett.* **2014**, *5*, 2791–2795.
- (66) Im, J.-H.; Chung, J.; Kim, S.-J.; Park, N.-G. Synthesis, Structure, And Photovoltaic Property Of A Nanocrystalline 2H Perovskite-Type Novel Sensitizer $(\text{CH}_3\text{CH}_2\text{NH}_3)\text{PbI}_3$. *Nanoscale Res. Lett.* **2012**, *7*, 353–353.
- (67) Stoumpos, C. C.; Malliakas, C. D.; Kanatzidis, M. G. Semiconducting Tin and Lead Iodide Perovskites with Organic Cations: Phase Transitions, High Mobilities, and Near-Infrared Photoluminescent Properties. *Inorg. Chem.* **2013**, *52*, 9019–9038.
- (68) Pellet, N.; Gao, P.; Gregori, G.; Yang, T.-Y.; Nazeeruddin, M. K.; Maier, J.; Grätzel, M. Mixed-Organic-Cation Perovskite Photo-

- voltaics for Enhanced Solar-Light Harvesting. *Angew. Chem., Int. Ed.* **2014**, *53*, 3151–3157.
- (69) Cheetham, A. K.; Rao, C. N. R.; Feller, R. K. Structural Diversity And Chemical Trends In Hybrid Inorganic–Organic Framework Materials. *Chem. Commun.* **2006**, *46*, 4780–4780.
- (70) Mitzi, D. B. Synthesis, Structure, and Properties of Organic–Inorganic perovskites and related materials. In *Progress in Inorganic Chemistry*; Karlin, K. D., Ed.; Wiley: Weinheim, Germany, 1999; Vol. 48, pp 1–121.
- (71) Ishihara, T. Optical-Properties of Pbi-Based Perovskite Structures. *J. Lumin.* **1994**, *60–1*, 269–274.
- (72) Dohner, E. R.; Hoke, E. T.; Karunadasa, H. I. Self-Assembly of Broadband White-Light Emitters. *J. Am. Chem. Soc.* **2014**, *136*, 1718–1721.
- (73) Dohner, E. R.; Jaffe, A.; Bradshaw, L. R.; Karunadasa, H. I. Intrinsic White-Light Emission from Layered Hybrid Perovskites. *J. Am. Chem. Soc.* **2014**, *136*, 13154–13157.
- (74) Sourisseau, S.; Louvain, N.; Bi, W.; Mercier, N.; Rondeau, D.; Boucher, F.; Buzare, J.-Y.; Legein, C. Reduced Band Gap Hybrid Perovskites Resulting From Combined Hydrogen And Halogen Bonding At The Organic–Inorganic Interface. *Chem. Mater.* **2007**, *19*, 600–607.
- (75) Knutson, J. L.; Martin, J. D.; Mitzi, D. B. Tuning The Band Gap In Hybrid Tin Iodide Perovskite Semiconductors Using Structural Templating. *Inorg. Chem.* **2005**, *44*, 4699–705.
- (76) Mercier, N.; Poiroux, S.; Riou, A.; Batail, P. Unique Hydrogen Bonding Correlating With A Reduced Band Gap And Phase Transition In The Hybrid Perovskites $(HO(CH_2)_2NH_3)_2PbX_4$ ($X = I, Br$). *Inorg. Chem.* **2004**, *43*, 8361–8366.
- (77) Mitzi, D. B. Synthesis, Crystal Structure, And Optical And Thermal Properties Of $(C_4H_9NH_3)_2MI_4$ ($M = Ge, Sn, Pb$). *Chem. Mater.* **1996**, *8*, 791–800.
- (78) Mercier, N.; Riou, A. An Organic–Inorganic Hybrid Perovskite Containing Copper Paddle-Wheel Clusters Linking Perovskite Layers: $Cu(O_2C(CH_2)_3NH_3)_2PbBr_4$. *Chem. Commun.* **2004**, *7*, 844–845.
- (79) Mitzi, D. B.; Chondroudis, K.; Kagan, C. R. Design, Structure, And Optical Properties Of Organic–Inorganic Perovskites Containing An Oligothiophene Chromophore. *Inorg. Chem.* **1999**, *38* (26), 6246–6256.
- (80) Mercier, N.; Louvain, N.; Bi, W. Structural Diversity And Retro-Crystal Engineering Analysis Of Iodometalate Hybrids. *CrystEngComm* **2009**, *11*, 720–734.
- (81) Smith, I. C.; Hoke, E. T.; Solis-Ibarra, D.; McGehee, M. D.; Karunadasa, H. I. A Layered Hybrid Perovskite Solar-Cell Absorber with Enhanced Moisture Stability. *Angew. Chem.* **2014**, *126*, 11414–11417.
- (82) Schmidt, L. C.; Pertegás, A.; González-Carrero, S.; Malinkiewicz, O.; Agouram, S.; Minguez Espallargas, G.; Bolink, H. J.; Galian, R. E.; Pérez-Prieto, J. Nontemplate Synthesis Of $CH_3NH_3PbBr_3$ Perovskite Nanoparticles. *J. Am. Chem. Soc.* **2014**, *136*, 850–3.
- (83) Todorov, T.; Gershon, T.; Gunawan, O.; Sturdevant, C.; Guha, S. Perovskite-Kesterite Monolithic Tandem Solar Cells With High Open-Circuit Voltage. *Appl. Phys. Lett.* **2014**, *105*, 173902–173902.
- (84) Lee, B.; Stoumpos, C. C.; Zhou, N.; Hao, F.; Malliakas, C. D.; Yeh, C.-Y.; Marks, T. J.; Kanatzidis, M. G.; Chang, R. P. H. Air Stable Molecular Semiconducting Iodosalts for Solar Cell Applications: Cs_2SnI_6 as a Hole Conductor. *J. Am. Chem. Soc.* **2014**, *136*, 15379–15385.
- (85) Nechache, R.; Harnagea, C.; Li, S.; Cardenas, L.; Huang, W.; Chakrabarty, J.; Rosei, F. Bandgap Tuning Of Multiferroic Oxide Solar Cells. *Nat. Photonics* **2014**, *9*, 61–67.
- (86) Guo, R.; You, L.; Zhou, Y.; Lim, Z. S.; Zou, X.; Chen, L.; Ramesh, R.; Wang, J. Non-Volatile Memory Based On The Ferroelectric Photovoltaic Effect. *Nat. Commun.* **2013**, *4*, 1990–1990.